

## Probabilistic tsunami hazard assessment with simulation-based response surfaces

T. Kotani<sup>a</sup>, K. Tozato<sup>b</sup>, S. Takase<sup>c</sup>, S. Moriguchi<sup>d,\*</sup>, K. Terada<sup>d</sup>, Y. Fukutani<sup>e</sup>, Y. Otake<sup>b</sup>, K. Nojima<sup>a</sup>, M. Sakuraba<sup>a</sup>, Y. Choe<sup>f</sup>

<sup>a</sup> Research and Development Center, Nippon Koei Co., Ltd. Inarihara, 2304, Tsukuba-shi, Ibaraki, 300-1259, Japan

<sup>b</sup> Department of Civil Engineering, Tohoku University, Aza-Aoba 468-1, Aramaki, Aoba-ku, Sendai, 980-0845, Japan

<sup>c</sup> Department of Civil Engineering and Architecture, Hachinohe Institute of Technology, 88-1 Ohbiraki, Myo, Hachinohe, Aomori, 031-8501, Japan

<sup>d</sup> International Research Institute of Disaster Science, Tohoku University, Aza-Aoba 468-1, Aramaki, Aoba-ku, Sendai, 980-0845, Japan

<sup>e</sup> College of Science and Engineering, Kanto Gakuin University, Mutsuura Higashi 1-50-1, Kanazawa-ku, Yokohama-shi, Kanagawa, 236-8501, Japan

<sup>f</sup> Department of Industrial and Systems Engineering, University of Washington, 3900 E Stevens Way NE, Seattle, WA, 98195, USA

### ARTICLE INFO

#### Keywords:

Probabilistic Tsunami hazard analysis  
Response surface  
Numerical simulations  
Uncertainty analysis  
Fault model

### ABSTRACT

This paper proposes a novel response surface-based method for probabilistic tsunami hazard assessment (PTHA). Although recent advancements in numerical simulation have enabled the accurate characterization of tsunami hazards, the high computational cost of numerical simulation often prohibits its broad application to probabilistic hazard analysis. The proposed method addresses this challenge by constructing the response surface (RS) of a target output using the results of high-fidelity tsunami simulations. The proposed method quantifies uncertainties in key simulation variables and propagates those uncertainties to the target output through the RS in a computationally efficient Monte Carlo simulation (MCS). We illustrate and validate the proposed method through a case study of the tsunami induced by the 2011 Great East Japan earthquake. The case study focuses on Sendai, Ishinomaki, and Kamaishi in Japan as the target locations. The proposed method estimates coastal tsunami heights while considering uncertainties in the fault slip and rake as well as the modeling error associated with the numerical simulation. The MCS allows us to estimate the probability density functions of the tsunami height at the target locations. The proposed method quantifies the contribution of each source of uncertainty to the overall uncertainty in the target output and thus facilitates engineering decision-making.

### 1. Introduction

Preparing for catastrophic natural hazards is a significant engineering challenge. The hardest part of this challenge is striking a balance between economy and safety; ensuring complete safety by structural measures incurs a prohibitive cost. To address this challenge, probabilistic approaches to evaluating such hazards and risks have been extensively discussed in the literature. In the field of seismic engineering, Cornell (1968) initiated an approach known as probabilistic seismic hazard analysis (PSHA). Subsequently, this approach has been studied by numerous researchers (e.g., McGuire, 1977; Anderson and Trifunac, 1978; Ishikawa and Kameda, 1988) and summarized in several reports and books (e.g., National Research Council, 1988; Working Group on California Earthquake Probabilities, 1995, 2002; McGuire, 2004).

Probabilistic tsunami hazard assessment (PTHA), which is based on

PSHA, enables us to quantitatively evaluate the probability of tsunami risks with a certain return period; it is one of the practical tools being used for disaster mitigation. Many studies on PTHA have been reported in the literature (e.g., Power et al., 2007; Thio et al., 2007; Burbidge et al., 2008; Mitsoudis et al., 2012; Suppasri et al., 2012; Stefanakis et al., 2014; Fukutani et al., 2015; Park and Cox, 2016; Griffin et al., 2016; Park et al., 2018; Park et al., 2019) and summarized in some review papers (e.g., Geist and Parsons, 2006; Behrens and Dias, 2015; Grezio et al., 2017; Mori et al., 2017). In particular, Annaka et al. (2007) proposed a very simple practical method that has been implemented successfully in PTHA handbooks currently used in Japan (Japan Society of Civil Engineers (JSCE) 2011; JNES 2014). In this method, uncertainties are classified into two types: *aleatory* uncertainties due to variations in actual phenomena and *epistemic* uncertainties due to insufficiencies in the knowledge, data, and modeling accuracy. Aleatory

\* Corresponding author.

E-mail address: [s\\_mori@irides.tohoku.ac.jp](mailto:s_mori@irides.tohoku.ac.jp) (S. Moriguchi).

uncertainties are estimated based on the results of case studies and numerical simulations, whereas epistemic uncertainties are often handled using a logic-tree approach (e.g. Annaka et al., 2007; Burbidge et al., 2008, Omira et al., 2016). The design standard published by the American Society of Civil Engineers (ASCE) is particularly important in this field. This standard (American Society of Civil Engineers, 2017) provides an extensive PTHA framework that is widely recognized as the first systematic PTHA framework. This framework (detailed in Sections 6.7 and C6.7 of the standard) provides a comprehensive guideline on determining inundation depths and flow velocities based on site-specific PTHA. This framework covers a broad range of uncertainties: epistemic uncertainties in model parameters (e.g., magnitude, fault depth, fault geometry, location, and slip distribution) and aleatory uncertainties (e.g., natural variability in source processes, modeling uncertainties, and tidal variation). By contrast, for illustration purposes, this paper's PTHA focuses on the uncertainties in two fault parameters (i.e., slip and rake) and the modeling error for the 2011 Great East Japan earthquake. Geographically, the ASCE standard covers Alaska, Hawaii, and the Pacific Coast of the U.S. concerning tsunami loads and effects. The standard recommends the use of 1) a statistically weighted logic tree approach to account for epistemic uncertainties and 2) probability distributions to account for aleatory uncertainties. For both types of uncertainties, this study uses probability distributions, as discussed later. While the standard provides detailed guidance on numerical simulations for PTHA (e.g., model spatial resolution), it does not directly advise on computational costs of PTHA. This paper addresses this gap by proposing a surrogate model-based computationally efficient way to perform PTHA.

Numerical simulations have also become essential tools for tsunami hazard assessment. Currently, these simulations are highly accurate thanks to recent advancements in computational mechanics (e.g., Larsen and Fuhrman, 2019; Sarfaraz and Park, 2016; Qin et al., 2018). However, numerical simulations are currently not being fully utilized in PTHA. Specifically, in the Japanese PTHA handbooks, the use of numerical simulations is restricted to obtaining the median value of the probability density function of the maximum tsunami height. The mean and standard deviation of the probability density function are estimated using a different empirical method proposed in the literature (e.g., Aida, 1978). However, considering recent advancements in tsunami simulations, we postulate that numerical simulations can be further used for PTHA. Hence, we propose a new method that effectively leverages numerical simulations for PTHA.

The novelty of the proposed method for PTHA lies in its use of the response surface (RS) of a target output, which is constructed based on the results of highly accurate tsunami simulations. Because tsunami simulations are computationally expensive, their direct use for comprehensive PTHA is computationally prohibitive. The current practice typically discretizes continuous probability distributions. For example, simulation runs are performed at 100 randomly chosen epicenter locations in a continuous geographic area (Mitsoudis et al., 2012); alternatively, probability masses are assigned to 72 tsunami scenarios to sparsely represent a continuous spectrum of scenarios (Park and Cox, 2016). This discretization makes PTHA computationally feasible at the expense of an approximation error. We address this challenge by using the RS as a surrogate model of the tsunami simulation model. The key idea is that the RS allows the continuous simulation output to be accurately approximated by interpolating/extrapolating outputs obtained at nearby inputs. Thus, once the important uncertainties are quantified (using empirical data, simulations, and engineering knowledge), an extensive Monte Carlo simulation (MCS) can be performed with the RS to stochastically evaluate possible hazards and risks. In our case study, we use only 50 numerical simulation runs to construct the RS, which is in turn evaluated 10,000 times with an MCS to perform comprehensive PTHA.

To demonstrate its capability, the proposed method is applied to a case study of the tsunami induced by the 2011 Great East Japan

earthquake. Our PTHA considers uncertainties in the fault slip and rake along with the modeling error in the numerical simulations. Sendai, Ishinomaki, and Kamaishi in Japan are selected as target study locations. The RS at each location is obtained based on numerical simulations of coastal tsunami heights. Finally, the probability density functions of the tsunami height are estimated by performing an extensive MCS. Furthermore, we quantify the contribution of each source of uncertainty to the overall uncertainty to determine the relative importance of each source for engineering decision-making. However, we note that the risk assessment exemplified in this study may not be directly applicable to other practical cases where additional sources of uncertainties should be taken into account. A main objective of this paper is to demonstrate the specific procedure of the proposed method and to discuss its capability and potential for practical applications.

## 2. Methodology

### 2.1. Fundamental scheme of the proposed method

In general, comprehensively evaluating the random field of a target output requires numerous simulation runs. Thus, using high-fidelity numerical simulations for this purpose is computationally expensive, if not infeasible. To address this problem, Honjo (2011) proposed a scheme, specifically for reliability-based design in geotechnical engineering. In this scheme, numerical simulations are carried out to obtain a RS that describes the trend of the target output subject to specific uncertainties. This scheme is highly efficient for performing a practical reliability assessment and is the basis of the PTHA method proposed in this study.

Fig. 1 shows the flowchart of the scheme proposed by Honjo (2011). The scheme consists of three phases: (i) geotechnical analysis, (ii) uncertainty analysis, and (iii) reliability assessment. In the *geotechnical analysis* phase, a series of simulations are performed for different calculation conditions and sets of input parameters. The results enable the construction of the RS in a later phase; this RS models the relationship between the target output  $Y$  and the set  $X$  of key variables such as important calculation conditions and input parameters. This process informs the analyst of how each variable in  $X$  influences the target output. The analyst also develops a sense of the physics and mechanisms governing the output  $Y$  by analyzing the simulation results based on his/her engineering knowledge and experience. In the *uncertainty analysis* phase, the uncertainties underlying  $X$  are quantified using databases and engineering knowledge. For example, if  $X$  is a set of quantitative variables, their probability distributions or general tendencies (e.g., average and standard deviation) should be determined. In contrast, if  $X$

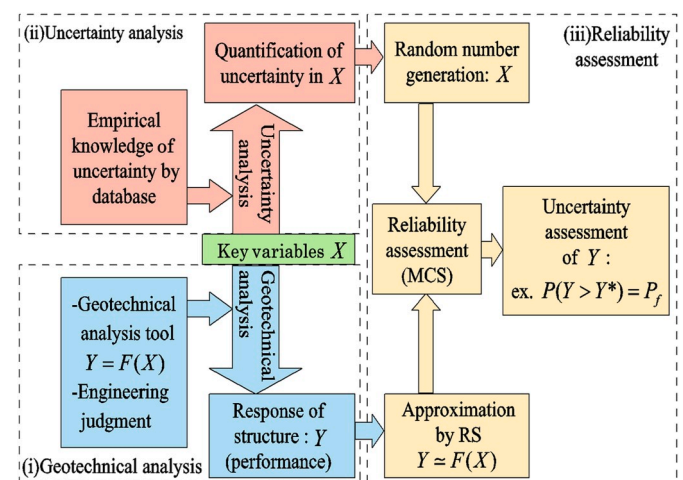


Fig. 1. Flowchart of the reliability-based design scheme proposed by Honjo (2011).

is a set of qualitative variables, the probabilities of observing qualitative events are required. If the uncertainties in  $X$  are all captured in databases, then quantifying the uncertainties in  $X$  is straightforward; however, in practice, it is usually necessary to rely on engineering judgments because of insufficient data. Finally, in the *reliability assessment* phase, the RS of the target output  $Y$  is constructed using the results of the geotechnical analysis. The RS is defined as a function of the key variables in  $X$  that describes the tendency of  $Y$  observed in the numerical simulations. Using the RS with the quantified uncertainties from the previous phase, a Monte Carlo simulation (MCS) is performed to obtain the probability density function of the target output  $Y$ . Because the RS is a surrogate model of the output, which is constructed based on the numerical simulations, the MCS results are expected to describe the same tendency observed in the numerical simulation results. Note that numerical simulation runs should be designed in careful consideration of the range of  $X$  because the RS aims to model the tendency of  $Y$  within, not beyond, the range of  $X$ .

2.2. Proposed PTHA method

In the reliability-based design scheme outlined in Section 2.1, the geotechnical analysis phase is separate from the other two phases. In this study, we propose replacing the geotechnical analysis phase with the tsunami analysis phase.

Fig. 2 shows the flowchart of the PTHA method proposed in this study. The proposed method first specifies the target output. The output can be quantitative such as the tsunami height, or qualitative, such as whether an area is flooded. Then, the method specifies the key variables, such as important input parameters and calculation conditions used in the tsunami analysis. The key variables should be determined based on numerical simulations. Specifically, we can vary variables that are expected to significantly influence the target output based on engineering knowledge and experience. It is efficient to determine the ranges of these key variables while observing how the variables affect the simulation outputs. Note that a large number of simulation runs is not necessary because the goal is simply to identify the tendency of the target output with respect to key variables.

There are two important uncertainties in numerical simulations, namely, *transformation error* and *modeling error*, according to Honjo (2011). The transformation error occurs when observational data are transformed into the input parameters of numerical simulations because the transformation is based on engineering assumptions and/or empirical knowledge. Although a discussion of the transformation error in

tsunami simulations would be interesting, this error is not taken into account in the present study. On the other hand, the modeling error captures the discrepancy between an empirical phenomenon and its numerical model; in other words, the modeling error represents the incompleteness of the model due to simplification and idealization and any inaccuracy due to discretization. This error is quantified in this study by comparing the simulated results with observational data.

The uncertainty analysis can be performed in parallel with the tsunami simulations. The analysis begins by gathering statistical information of the key variables. This information (e.g., mean, variance, and distribution type) is used to determine the probability distributions of the key variables.

Subsequently, the reliability assessment is performed based on the results of the tsunami simulations and uncertainty analysis. Using the tsunami simulation results, an RS is constructed as an approximate function  $Y \approx F(X)$ . Note that the effects of bathymetry and topography are represented directly in the tsunami simulations and hence are also reflected in the RS. Then, we perform an MCS for the reliability assessment using the RS and the probability distributions of the key variables.

Some related studies in the literature (e.g. Sarri et al., 2012; Sraj et al., 2014; Omira et al., 2015; Lorito et al., 2015; Selva et al., 2016; Volpe et al., 2019) also statistically analyze simulation results to reduce the total computational cost of PTHA. These studies, however, do not consider the modeling error of numerical simulations. To the best of our knowledge, this study is the first to quantify the effect of the modeling error in comparison to other uncertainties.

3. Application

3.1. Target output

In this section, a case study is presented to illustrate the specific procedure of the proposed RS-based PTHA method and validate its capability. This case study concerns the tsunami induced by the 2011 Great East Japan earthquake. We specified the tsunami height as the target output, and the proposed PTHA method was used to evaluate the tsunami heights at three coastal locations in Japan—Kamaishi, Sendai, and Ishinomaki (see Fig. 3). These locations are close to the coastline with water depths of 10–20 m. While this study focuses on the tsunami heights along the coastline as the target outputs for illustration purposes, future work can also use the proposed method to study tsunami runups.

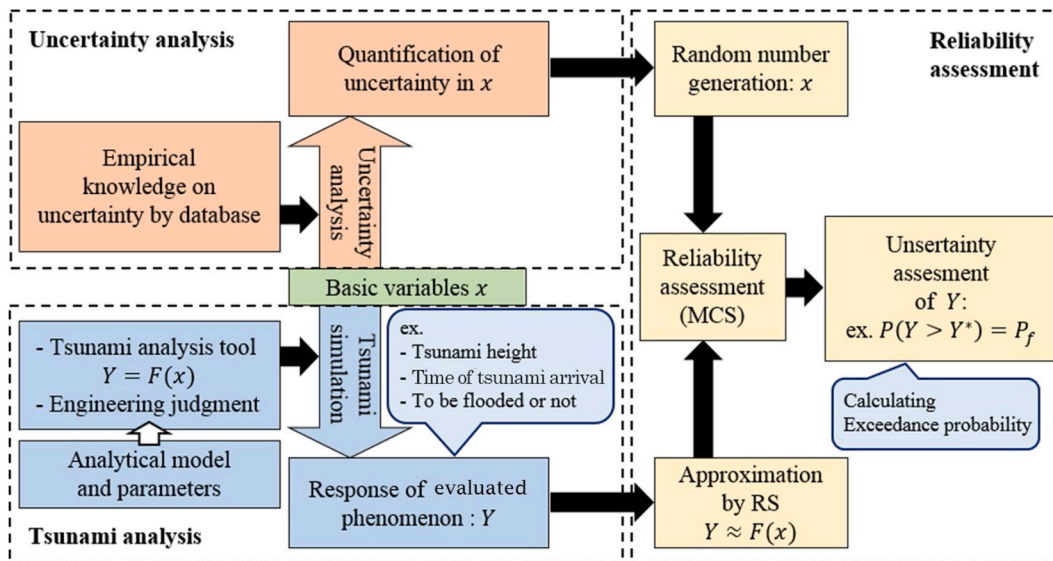


Fig. 2. Flowchart of the proposed RS-based PTHA method.

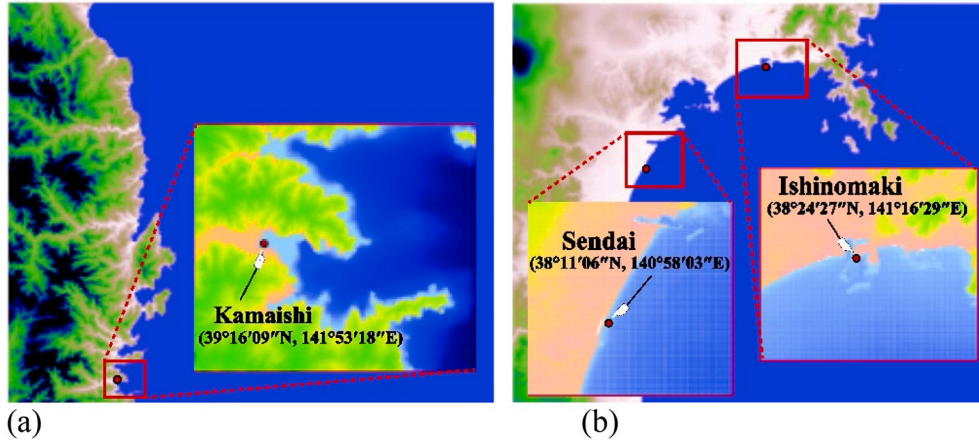


Fig. 3. Measurement points for the tsunami heights: (a) Kamaishi, (b) Sendai, and Ishinomaki.

3.2. Step (i): Tsunami analysis

3.2.1. Uncertainty in the tsunami hazard

Various phenomena characterize a tsunami (e.g., initial uplift of the sea surface induced by fault movement, followed by propagation and runup), each with its own uncertainty. Because it is impractical to incorporate all possible uncertainties into a model, it is necessary to select and model the key uncertainties. The fault model is recognized as the most widely used model in tsunami analysis (Kajiura, 1963, 1982). Various fault parameters, including the fault slip and rake, are illustrated in Fig. 4. A JSCE committee summarized the influence of each fault parameter on the tsunami height (Japan Society of Civil Engineers, 2002). Based on previous studies, we selected the fault slip and rake as the two key variables in this study. To calculate the fault displacement, we used the Fujii–Satake model Ver. 8.0 (FS55v80) (Satake et al., 2013), which is one of the most widely used fault models for the 2011 Great East Japan earthquake (see Fig. 5). This model considers 55 subfaults and provides the spatial slip distribution. According to Goda et al. (2014), this model’s tsunami predictions “agree well with the tsunami observations.”

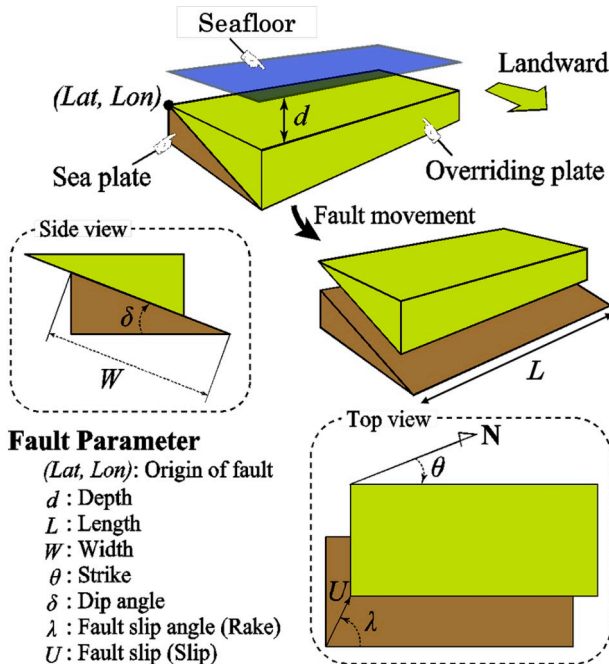


Fig. 4. Illustration of the fault parameters.

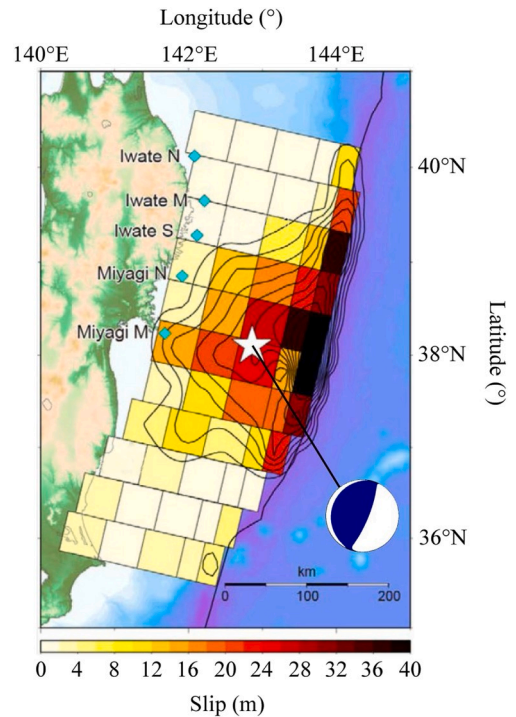


Fig. 5. Fujii–Satake model Ver. 8.0 (FS55v80) and the result of a centroid moment tensor (CMT) inversion (after Satake et al., 2013).

3.2.2. Calculation conditions and governing equations

As explained in the previous subsection, the Fujii–Satake model Ver. 8.0 (FS55v80) considers 55 subfaults. We varied the slip and rake values in the tsunami simulation to assess their effects on the target output. As summarized in Table 1, we considered 50 test cases based on 5 slip values and 10 rake values to cover reasonable ranges of the parameters. The slip and rake values used in case S3R5 are the same as the original parameters of FS55v80. The other calculation conditions are given in Table 2. The initial distribution of the tsunami height relative to the standard sea level in Japan (Tokyo Peil) was obtained using the method proposed by Okada (1992), in which the vertical sea-surface displacement is calculated using a fault model. To describe tsunami propagation, the following continuity equation (1) and nonlinear shallow water equations (2) and (3) were used:

$$\frac{\partial \eta}{\partial t} + \frac{\partial M}{\partial x} + \frac{\partial N}{\partial y} = 0 \tag{1}$$

**Table 1**  
Calculation cases..

		Rake										
		[°]	-20	-15	-10	-5	0	+5	+10	+15	+20	+25
	Normalized value		0.753	0.815	0.877	0.938	1	1.062	1.123	1.185	1.247	1.309
Slip	70	0.7	S1R1	S1R2	S1R3	S1R4	S1R5	S1R6	S1R7	S1R8	S1R9	S1R10
	85	0.85	S2R1	S2R2	S2R3	S2R4	S2R5	S2R6	S2R7	S2R8	S2R9	S2R10
	100	1	S3R1	S3R2	S3R3	S3R4	S3R5	S3R6	S3R7	S3R8	S3R9	S3R10
	120	1.2	S4R1	S4R2	S4R3	S4R4	S4R5	S4R6	S4R7	S4R8	S4R9	S4R10
	140	1.4	S5R1	S5R2	S5R3	S5R4	S5R5	S5R6	S5R7	S5R8	S5R9	S5R10

**Table 2**  
Calculation conditions.

Item	Note
Scenario	Tsunami hazard of the 2011 Great East Japan earthquake
Fault model	Fujii-Satake model Ver. 8.0
Initial waveform	Calculate crustal deformation and sea-surface displacement using the method of Okada (1992)
Governing equations	Nonlinear shallow water equations
Calculation scheme	Leapfrog method and staggered grids
Computational grid interval (with nesting)	Domain 1: 2430 m; Domain 2: 810 m; Domain 3: 270 m; Domain 4: 90 m
Boundary conditions	Offshore boundary: transmitting boundary Landward boundary: reflecting boundary
Tidal level	Set at Tokyo Peil (T.P.) -0.57 m (coseismic tidal level)
Calculation time	180 min from earthquake generation

$$\frac{\partial M}{\partial t} + \frac{\partial}{\partial x} \left[ \frac{M^2}{D} \right] + \frac{\partial}{\partial y} \left[ \frac{MN}{D} \right] + gD \frac{\partial \eta}{\partial x} + \frac{gn^2}{D^{3/2}} M \sqrt{M^2 + N^2} = 0 \quad (2)$$

$$\frac{\partial N}{\partial t} + \frac{\partial}{\partial x} \left[ \frac{MN}{D} \right] + \frac{\partial}{\partial y} \left[ \frac{N^2}{D} \right] + gD \frac{\partial \eta}{\partial y} + \frac{gn^2}{D^{3/2}} N \sqrt{M^2 + N^2} = 0 \quad (3)$$

where  $\eta$  is the vertical displacement of the water surface;  $D$  is the total water depth;  $g$  is the acceleration due to gravity;  $n$  is the Manning coefficient; and  $M$  and  $N$  are the fluxes in the  $x$  and  $y$  directions, respectively. The governing equations were discretized using the staggered leapfrog scheme (Goto and Ogawa, 1982; Goto et al., 1997). The calculation grids were generated as shown in Fig. 6 according to Imaura et al. (2006). The computational domain was divided into calculation grids that were nested from the wave source to the target locations

with grid intervals of 2430, 810, 270, and 90 m. For the area covered with grids of intervals 2430–270 m, ETOPO1 digital elevation data (Amante and Eakins, 2009) were used for the topographical conditions. For the area covered with a grid interval of 90 m, we used digital elevation data from the Digital 10 m Grid Elevation Map published by the Geospatial Information Authority of Japan. We also used the M7000 series of isobathic data (JapanHydrographic Association, 2015), which are high-resolution seafloor topography data. The reflecting boundary condition was used on the coastline.

3.2.3. Simulation results

We began by checking the validity of the tsunami analysis model used in this study. As explained in Section 3.2.2, the conditions of calculation case S3R5 correspond to those of FS55v80. It is therefore possible to compare the S3R5 results with the empirical data of the 2011 Great East Japan earthquake. The time histories of the wave heights at the five offshore points indicated in Fig. 5 were used as the observational data, as shown in Fig. 7. These data were collected by GPS wave recorders of the Nationwide Ocean Wave Information Network for Ports and Harbours (The Port and Airport Research Institute, 2011). As seen in Fig. 7, the simulation results generally match the observational data at the five offshore points. Any discrepancies represent the modeling error discussed in Section 2.2. Section 3.3.1 will detail how we quantified the modeling error. Note that because observational data are subject to measurement errors, the modeling error is also affected by measurement errors.

The spatial distributions of the maximum tsunami height were determined within 180 min after tsunami generation, and the results are shown in Fig. 8. Additionally, the maximum tsunami heights at Sendai, Ishinomaki, and Kamaishi are summarized in Table 3 for the 50 cases. These results indicate that fault slip is the dominant parameter at all locations.

3.3. Step (ii): Uncertainty analysis

3.3.1. Quantification of uncertainties in key variables

Uncertainties in key variables, represented as probability distributions, are important inputs for the MCS. To specify the probability distributions, we can use statistical information such as the average  $\mu$ , standard deviation  $\sigma$ , and probability distribution type. There are two approaches to obtain this information: 1) estimation based on empirical data and 2) estimation based on engineering judgment and knowledge.

In this study, we employed the former approach for the modeling error and the latter approach for the fault parameters (slip and rake). Table 4 shows the estimated statistical values for the key variables.

In this study, normal distributions were used to represent epistemic

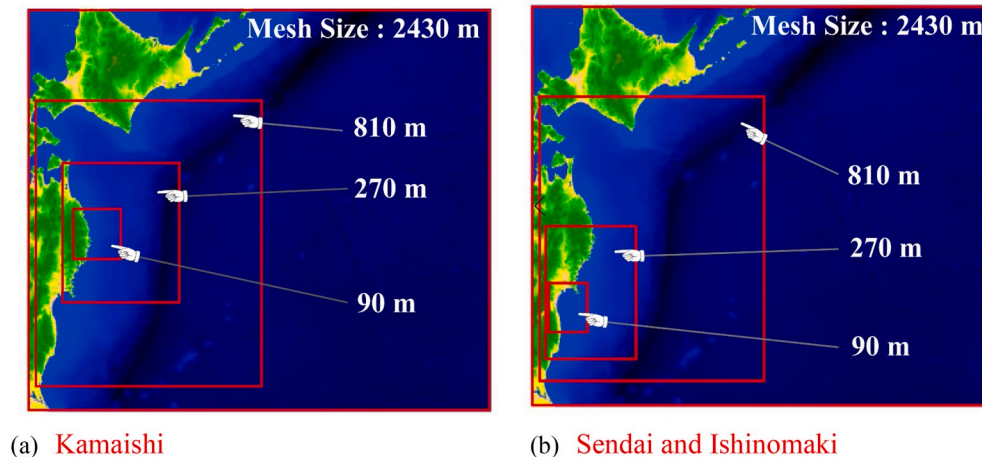
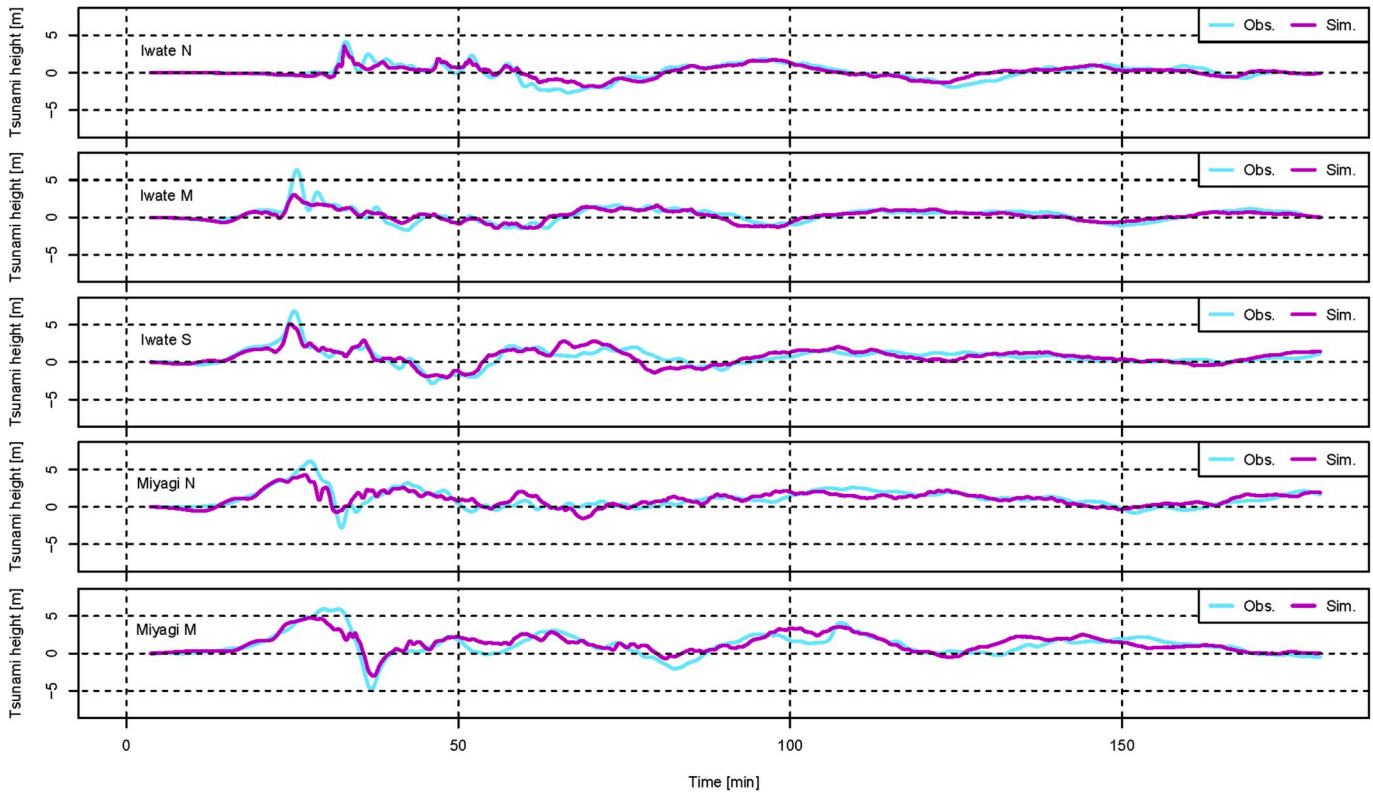


Fig. 6. Nested analysis regions.



**Fig. 7.** Comparison between the observational data and simulation results at the offshore points shown in Fig. 5 (Observational data: Nationwide Ocean Wave Information Network for Ports and Harbors (The Port and Airport Research Institute, 2011)).

uncertainties in the fault parameters (slip and rake). While the best distribution for the slip may be right heavy-tailed according to an in-depth study on the 2011 Great East Japan earthquake (Goda et al., 2014), our use of a normal distribution serves to illustrate how to implement the proposed procedure when there is little to no empirical knowledge of the fault parameters. The choice of a normal distribution is justified according to the principle of maximum entropy when we can specify only the mean and variance of a continuous distribution to represent epistemic uncertainty (Dowson and Wragg, 1973).

As mentioned in Section 3.2.2, the slip and rake values of each subfault were expressed as ratios with respect to the original FS55V80 parameters. Thus, the values were normalized (see Table 1), and the average slip and rake values were set as 1.0. Based on the moment magnitude scale  $M_w$ , the slip and rake standard deviations were specified as 0.1 and 0.04, respectively. According to Kanamori (1977),  $M_w$  is related to the slip  $D$  as follows:

$$\log_{10} M_0 = 1.5M_w + 9.1, \quad (4)$$

$$M_0 = rDS, \quad (5)$$

where  $M_0$  is the seismic moment,  $r$  is the rigidity, and  $S$  is the fault area. Hanks and Kanamori (1979) proposed a modified relationship, but the original version, which is still widely accepted, is used in this study. As reported by Japan Society of Civil Engineers (2011), the estimated standard deviation of  $M_w$  of an earthquake having the same magnitude as the 2011 Great East Japan earthquake is approximately 0.1. Using this value, the range of values of the normalized slip becomes 0.71–1.41. Because the range of a normal distribution is approximately  $\pm 3\sigma$ , a slip standard deviation of 0.1 was used to cover the range of 0.71–1.41. The rake standard deviation was determined similarly. Japan Society of Civil Engineers (2011) conducted calculations with different rake values and reported that  $\pm 10^\circ$  is a suitable rake range; this range becomes 0.9–1.1 upon normalization. Therefore, a rake standard deviation of 0.04 was

used to cover this range.

The modeling error of the numerical simulation was also considered one of the uncertainties. The time histories shown in Fig. 7 were used to quantify the modeling error  $M_{\text{err}}$ , which is defined as the difference between the observed tsunami height  $H_{\text{obs}}$  and the simulated tsunami height  $H_{\text{sim}}$ :

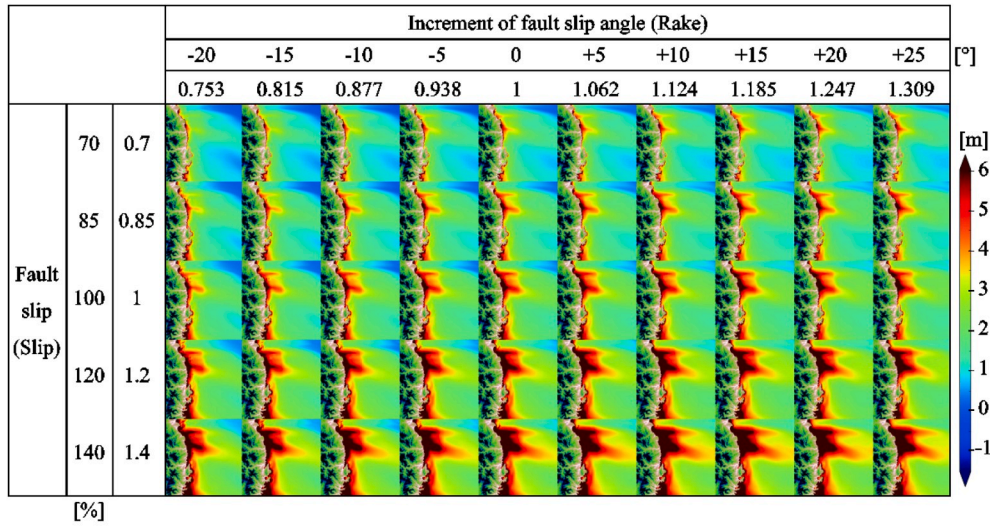
$$M_{\text{err}} = H_{\text{obs}} - H_{\text{sim}}. \quad (6)$$

Because we possessed time histories from both simulations and observations, the modeling error was quantified at numerous times. Fig. 9 shows a histogram of the modeling error showing that the modeling error can be represented as a normal distribution with an average and standard deviation of approximately 0.49 and 0.76 m, respectively. Note that there are some limitations on the modeling error considered in this study; we considered only the time histories of the tsunami height at offshore points and did not take other effects into account. For instance, the rigid boundary conditions along the coastline have effects that should be considered. Other available information, such as tsunami runups and inundation areas, may be considered in future work. Additionally, note that in this study, a normal distribution was assumed to roughly capture the tendency of the modeling error. However, in general, when choosing distributions to describe uncertainties, users of the proposed procedure would want to consider various parametric distributions (e.g., a skew-normal distribution to better describe the positive skewness observed in the modeling error depicted in Fig. 9) as well as nonparametric distributions if the data size is sufficiently large.

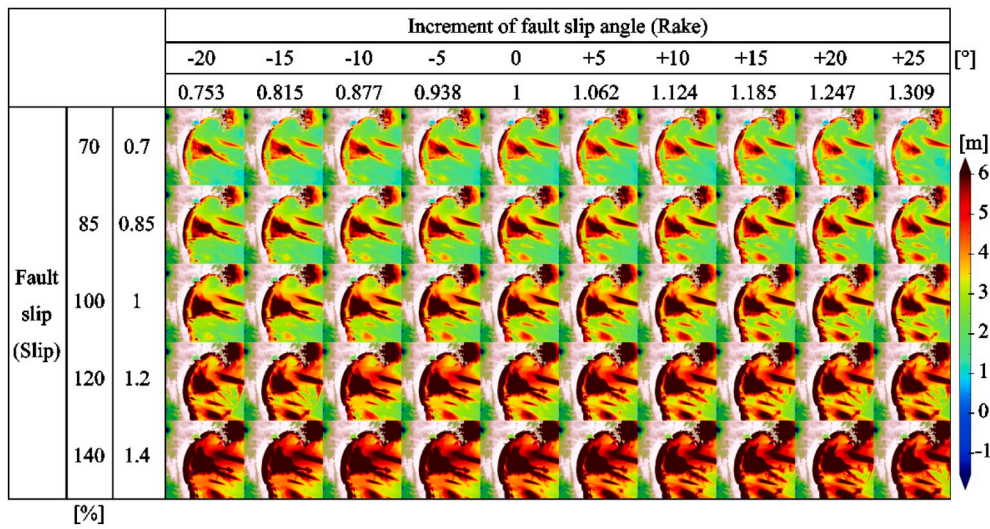
### 3.4. Step (iii): Reliability assessment

#### 3.4.1. Construction of the response surface

The RS of the tsunami height was constructed using the tsunami simulation results in Table 3. In this study, the slip and rake were selected as the independent variables of the RS. The RSs at the three



(a)



(b)

Fig. 8. Spatial distributions of the maximum tsunami height for each calculation: (a) 90-m mesh shown in Fig. 6(a) and (b) 90-m mesh shown in Fig. 6(b).

target locations (Sendai, Ishinomaki, and Kamaishi) were constructed separately because their responses were sufficiently different from each other. Prior to constructing the RSs, we investigated the tendency of each response with respect to each independent variable. From this investigation, we confirmed a linear relationship between the tsunami height and the slip and a nonlinear relationship between the tsunami height and the rake. These tendencies agree with the findings in relevant studies (Necmioglu and Ozel, 2014; Goda et al., 2014). Therefore, we added a quadratic term in the rake to the RSs. Additionally, a slip–rake cross term was included. The resulting form of the RS is

$$H_{max} = aU + b\lambda + cU\lambda + d\lambda^2 + e, \tag{7}$$

where  $H_{max}$  is the tsunami height,  $U$  is the slip,  $\lambda$  is the rake, and  $a, b, c, d,$  and  $e$  are undetermined coefficients. Note that the modeling error is not included in Eq. (7). The coefficients were determined by fitting the results in Table 3. There are four terms that include the independent RS variables, and we considered 15 forms of RSs (all  $2^4$  forms except the constant RS).

In general, we can use forward selection, backward elimination, stepwise methods, or other variable selection methods to optimize the

RS efficiently for numerous independent variables. However, because of the relatively modest number of terms considered in this study, we checked every functional form using multiregression analysis. Tables 5–7 show the fitted value of each coefficient, the adjusted  $R^2$  value, the residual standard error (r.s.e.), and the value of the Akaike information criterion (AIC) (Akaike, 1973) of the RS for each of the three target locations in Fig. 3. We selected the functional form with the lowest AIC value as the most suitable one. As a result, the same functional form was selected coincidentally for Sendai, Ishinomaki, and Kamaishi. The selected forms are highlighted in boldface in Tables 5–7. The fact that the same functional form was selected for all the target locations means that the dominant terms were identical independent of location. The constructed RS for each target location is shown in Fig. 10, where the blue surface is constructed from the red points obtained from the numerical simulations (see Table 3). Because a visual inspection of Fig. 10 confirms that the variation in each RS is small between adjacent red points, the number of simulation runs seems sufficient. Note that determining the optimal design of computational experiments to build a surrogate model such as an RS is an active research topic in statistics (e.g., Stefanakis et al., 2014).

**Table 3**  
Maximum tsunami heights for the 50 cases at Sendai, Ishinomaki, and Kamaishi.

Case	Slip	Rake	Tsunami height [m]		
			Sendai	Ishinomaki	Kamaishi
S1R1	0.700	0.735	7.695	4.226	10.003
S1R2	0.700	0.815	7.880	4.443	9.950
S1R3	0.700	0.877	7.911	4.626	9.845
S1R4	0.700	0.938	7.808	4.780	9.693
S1R5	0.700	1.000	7.759	4.897	9.484
S1R6	0.700	1.062	7.590	4.982	9.210
S1R7	0.700	1.124	7.496	5.033	8.951
S1R8	0.700	1.185	7.266	5.049	8.593
S1R9	0.700	1.247	6.974	5.034	8.197
S2R10	0.700	1.309	6.745	4.981	7.714
S2R1	0.850	0.735	9.296	5.036	11.803
S2R2	0.850	0.815	9.309	5.295	11.724
S2R3	0.850	0.877	9.255	5.516	11.571
S2R4	0.850	0.938	9.273	5.694	11.345
S2R5	0.850	1.000	9.272	5.834	11.077
S2R6	0.850	1.062	8.986	5.927	10.757
S2R7	0.850	1.124	8.702	5.982	10.369
S2R8	0.850	1.185	8.481	5.994	9.962
S2R9	0.850	1.247	8.285	5.975	9.537
S2R10	0.850	1.309	7.877	5.919	9.046
S3R1	1.000	0.735	10.587	5.824	13.476
S3R2	1.000	0.815	10.805	6.125	13.382
S3R3	1.000	0.877	10.658	6.384	13.210
S3R4	1.000	0.938	10.612	6.598	12.956
S3R5	1.000	1.000	10.654	6.762	12.681
S3R6	1.000	1.062	10.281	6.878	12.308
S3R7	1.000	1.124	10.205	6.943	11.828
S3R8	1.000	1.185	9.859	6.954	11.334
S3R9	1.000	1.247	9.370	6.907	10.737
S3R10	1.000	1.309	9.107	6.824	10.160
S4R1	1.200	0.735	12.402	6.827	15.770
S4R2	1.200	0.815	12.735	7.185	15.672
S4R3	1.200	0.877	12.732	7.487	15.468
S4R4	1.200	0.938	12.662	7.744	15.161
S4R5	1.200	1.000	12.603	7.942	14.836
S4R6	1.200	1.062	12.331	8.085	14.396
S4R7	1.200	1.124	11.926	8.171	13.826
S4R8	1.200	1.185	11.513	8.211	13.257
S4R9	1.200	1.247	11.119	8.169	12.537
S4R10	1.200	1.309	10.511	8.064	11.775
S5R1	1.400	0.735	14.454	7.830	18.282
S5R2	1.400	0.815	14.410	8.226	18.099
S5R3	1.400	0.877	14.581	8.552	17.827
S5R4	1.400	0.938	14.582	8.823	17.516
S5R5	1.400	1.000	14.434	9.057	17.109
S5R6	1.400	1.062	14.287	9.226	16.520
S5R7	1.400	1.124	13.875	9.338	15.906
S5R8	1.400	1.185	13.325	9.384	15.204
S5R9	1.400	1.247	12.575	9.366	14.438
S5R10	1.400	1.309	12.041	9.263	13.553

**Table 4**  
Statistical information on the fault slip, rake, and modeling error.

Basic variables	Average value	Standard deviation	Distribution function type
Slip	1.0	0.1	Normal distribution
Rake	1.0	0.04	Normal distribution
Modeling error	0.487	0.758	Normal distribution

The results show that the slip affects the tsunami height more than the rake does. This is in accordance with the findings reported in the literature. Although the tsunami height decreases with increasing rake at both Sendai and Kamaishi, the opposite tendency is seen at Ishinomaki. We reason that this difference is due to the positional relationship between the locations of cities and the directions of tsunami propagation. Because the direction of the coastline at Ishinomaki is different from those at the other two cities, the rake would have a different effect.

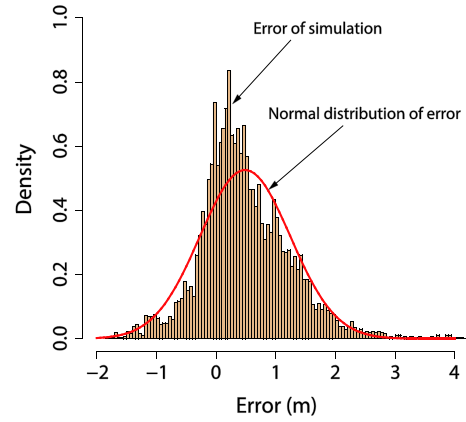


**Fig. 9.** Histogram of the modeling error approximated by a normal distribution.

The modeling error is considered in each RS by adding Eq. (6) to Eq. (7). Hence, the final form of the RS is as follows:

$$H_{max} = aU + b\lambda + cU\lambda + d\lambda^2 + e + M_{err} \quad (8)$$

The resulting RSs are used for the MCS in the next section.

### 3.4.2. Monte Carlo simulation

The MCS was performed using the RSs and the probability distributions of the key variables from the previous sections. Specifically, we first generated the values of the key variables (slip, rake, and modeling error) from the probability distributions. Using these values as inputs to the RSs, we evaluated the tsunami height at each target location. Using 10,000 replications, we then estimated the probability density function of the tsunami height.

### 3.4.3. Probability density of the tsunami height

Fig. 11 shows the estimated probability density function of the tsunami height at each target location. Using the density function, we can estimate the exceedance probability for any tsunami height. In this study, as a validation of the proposed method, the tsunami height observed at each target location for the 2011 Great East Japan earthquake was used to estimate the exceedance probability; hence, the theoretical exceedance probability should be 50%.

The tsunami heights observed at the target locations are summarized in Table 8. These heights were derived from tsunami trace height data collected in a field survey (Mori and Takahashi, 2012), from which we used the tsunami trace height reported at the survey point closest to each target location except for Sendai; because three survey points were located near the target location for Sendai, the average tsunami trace height was used. The tsunami heights estimated from the field survey and the calculated exceedance probability are shown in Fig. 11. For Sendai and Ishinomaki, the median values are close to the results of the field survey. For Kamaishi, the median value seems much larger than the field survey result (the exceedance probability is 91%). However, we note that their absolute difference is 1.5 m, which is only approximately 10–15% of the field survey result. Because our numerical simulation used the perfect reflecting boundary condition despite the complex shape of the coastline near Kamaishi, we attribute this relatively large deviation to a wave amplification effect near the coastline.

### 3.4.4. Calculation of contribution ratios

The variance of the probability density function of a target output can be apportioned between multiple sources of uncertainties. It is practically important to analyze the sensitivity of the target output with respect to each uncertainty. In this section, the contribution ratio  $R_i$  of each uncertainty (i.e., in the slip, rake, and modeling error) is quantified as follows:

**Table 5**  
Response surface for Sendai.

No.	Coefficients of each term					R <sup>2</sup>	r.s.e. [m]	AIC
	a	b	c	d	e			
	(t-value)							
1	<b>12.4757 (29.684)</b>	<b>20.2928 (14.665)</b>	<b>-3.3048 (-8.225)</b>	<b>-9.6583 (-15.124)</b>	<b>-9.1908 (-11.561)</b>	<b>0.997</b>	<b>0.125</b>	<b>-59.30</b>
2		8.1858 (1.380)	8.4496 (27.649)	-9.6583 (-3.371)	3.6591 (1.223)	0.944	0.561	89.92
3	10.6590 (11.162)		-1.5426 (-1.692)	-0.7472 (-1.600)	1.9786 (3.653)	0.984	0.297	26.41
4	9.0688 (81.347)	16.8888 (8.173)		-9.6583 (-9.664)	-5.6817 (-5.412)	0.993	0.196	-15.42
5	12.4757 (12.169)	0.3800 (0.366)	-3.3048 (-3.372)		0.7693 (0.708)	0.983	0.305	28.98
6			8.4719 (-21.45)	-5.7217 (27.50)	7.7667 (26.03)	0.942	0.566	89.95
7	9.0688 (52.51)			-1.5135 (-12.94)	2.8170 (12.62)	0.984	0.303	27.43
8	9.0688 (47.23)	-3.0240 (-11.25)			4.2784 (12.45)	0.980	0.337	38.09
9		-11.7271 (-19.40)	8.4496 (25.03)		13.6193 (26.34)	0.931	0.620	98.96
10		16.889 (0.686)		-9.658 (-0.812)	3.659 (0.295)	0.026	2.330	231.37
11	12.1162 (41.648)		-2.9562 (-12.995)		1.1611 (6.365)	0.984	0.302	27.12
12				-1.5135 (-1.693)	12.1578 (11.789)	0.037	2.317	229.87
13	9.0688 (24.837)				1.1611 (3.001)	0.926	0.640	101.35
14		-3.024 (-1.633)			13.619 (7.032)	0.033	2.321	230.07
15			4.6807 (5.707)		5.5320 (6.086)	0.392	1.841	206.87

**Table 6**  
Response surface for Ishinomaki.

No.	Coefficients of each term					R <sup>2</sup>	r.s.e. [m]	AIC
	a	b	c	D	e			
	(t-value)							
1	<b>3.9609 (25.30)</b>	<b>12.9900 (25.20)</b>	<b>1.8460 (12.33)</b>	<b>-6.2871 (-26.42)</b>	<b>-5.7844 (-19.53)</b>	<b>0.9991</b>	<b>0.04658</b>	<b>-158.03</b>
2		9.14613 (4.811)	5.57792 (56.970)	-6.28714 (-6.848)	-1.70469 (-1.778)	0.9861	0.1797	-23.90
3	2.7980 (4.864)		2.9741 (5.416)	-0.5829 (-2.071)	1.3654 (4.184)	0.9862	0.1791	-24.27
4	5.86388 (106.74)	14.89138 (14.62)		-6.28714 (-12.77)	-7.74449 (-14.97)	0.996	0.09641	-86.19
5	3.96092 (6.293)	0.02763 (0.043)	1.84598 (3.068)		0.69916 (1.048)	0.9849	0.1872	-19.81
6			5.6029 (47.24)	-1.8887 (-18.39)	2.8848 (25.11)	0.9795	0.218	-5.52
7	5.86388 (45.393)			0.89442 (10.227)	-0.25095 (-1.503)	0.9778	0.22678	-1.60
8	5.8639 (50.62)	1.9290 (11.90)			-1.2609 (-6.08)	0.9822	0.2033	-12.51
9		-3.8163 (-15.49)	5.5779 (40.52)		4.7789 (22.67)	0.9725	0.2527	9.24
10		14.891 (0.937)		-6.287 (-0.818)	-1.705 (-0.213)	0.02497	1.504	187.62
11	3.9348 (22.062)		1.8713 (13.419)		0.7276 (6.507)	0.9852	0.1852	-21.81
12				0.8944 (1.543)	5.7888 (8.657)	0.02743	1.502	186.55
13	5.8639 (25.543)				0.7276 (2.992)	0.93	0.4029	54.94
14		1.929 (1.613)			4.779 (3.821)	0.03168	1.499	186.33
15			4.3514 (15.81)		2.1471 (7.04)	0.8356	0.6177	97.68

**Table 7**  
Response surface for Kamaishi.

No.	Coefficients of each term					R <sup>2</sup>	r.s.e. [m]	AIC
	a	b	c	d	e			
	(t-value)							
1	<b>16.8426 (63.57)</b>	<b>18.4973 (21.21)</b>	<b>-6.2884 (-24.83)</b>	<b>-8.8271 (-21.93)</b>	<b>-7.5201 (-15.01)</b>	<b>0.9992</b>	<b>0.07881</b>	<b>-105.44344</b>
2		2.1523 (0.274)	9.5804 (23.676)	-8.8271 (-2.326)	9.8278 (2.481)	0.932	0.7428	117.99572
3	15.1866 (18.293)		-4.6821 (-5.907)	-0.7045 (-1.735)	2.6610 (5.650)	0.9918	0.2584	12.41913
4	10.3600 (60.840)	12.0202 (3.808)		-8.8271 (-5.783)	-0.8431 (-0.526)	0.989	0.2988	26.94284
5	16.8426 (18.803)	0.2982 (0.329)	-6.2884 (-7.344)		1.5829 (1.668)	0.9913	0.2665	15.46987
6			9.5863 (23.96)	-7.7920 (-22.49)	10.9078 (28.15)	0.9333	0.7355	116.07724
7	10.3600 (53.62)			-3.0302 (-23.17)	5.2057 (20.84)	0.9858	0.3391	38.64625
8	10.3600 (46.80)	-6.1789 (-19.94)			8.2599 (20.84)	0.9814	0.3885	52.26004
9		-16.0467 (-21.18)	9.5804 (22.64)		18.9307 (29.20)	0.9256	0.7769	121.55742
10		12.020 (0.427)		-8.827 (-0.648)	9.828 (0.691)	0.1226	2.669	244.95227
11	16.5605 (65.17)		-6.0148 (-30.27)		1.8903 (11.86)	0.9914	0.2639	13.58715
12				-3.030 (-2.969)	15.876 (13.481)	0.1375	2.646	243.14541
13	10.3600 (15.377)				1.8903 (2.648)	0.8277	1.182	162.60447
14		-6.179 (-2.921)			18.931 (8.555)	0.1332	2.652	243.39644
15			4.423 (3.977)		7.865 (6.380)	0.2322	2.496	237.33548

$$R_i = \frac{\sigma_i^2}{\sigma_{all}^2} \times 100 [\%], \tag{9}$$

where  $\sigma_i^2$  is the variance of the probability density function based only

on the uncertainty  $i$  and  $\sigma_{all}^2$  is the variance based on all the uncertainties. The results obtained from Eq. (9) for each target location are given in Table 9. For Sendai and Kamaishi, the contribution ratio of slip is approximately 60%, and that of the modeling error is approximately

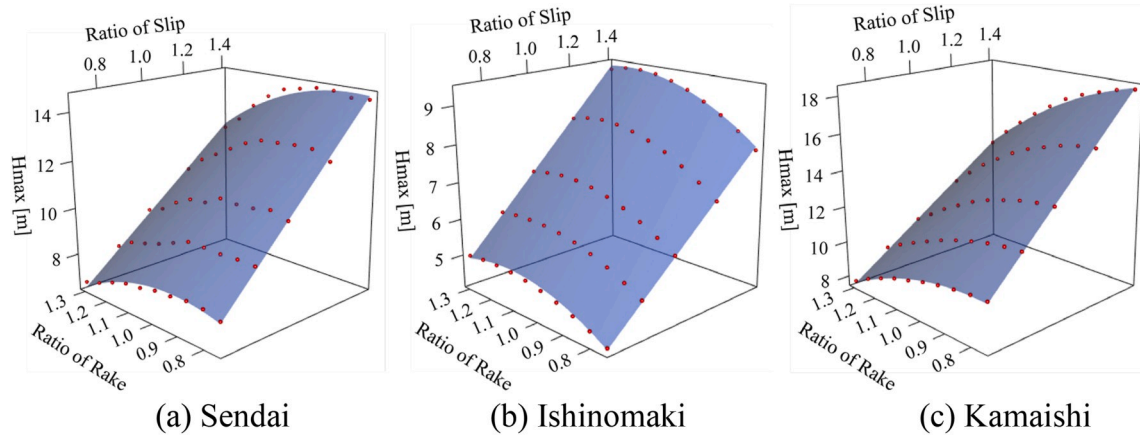


Fig. 10. Response surfaces.

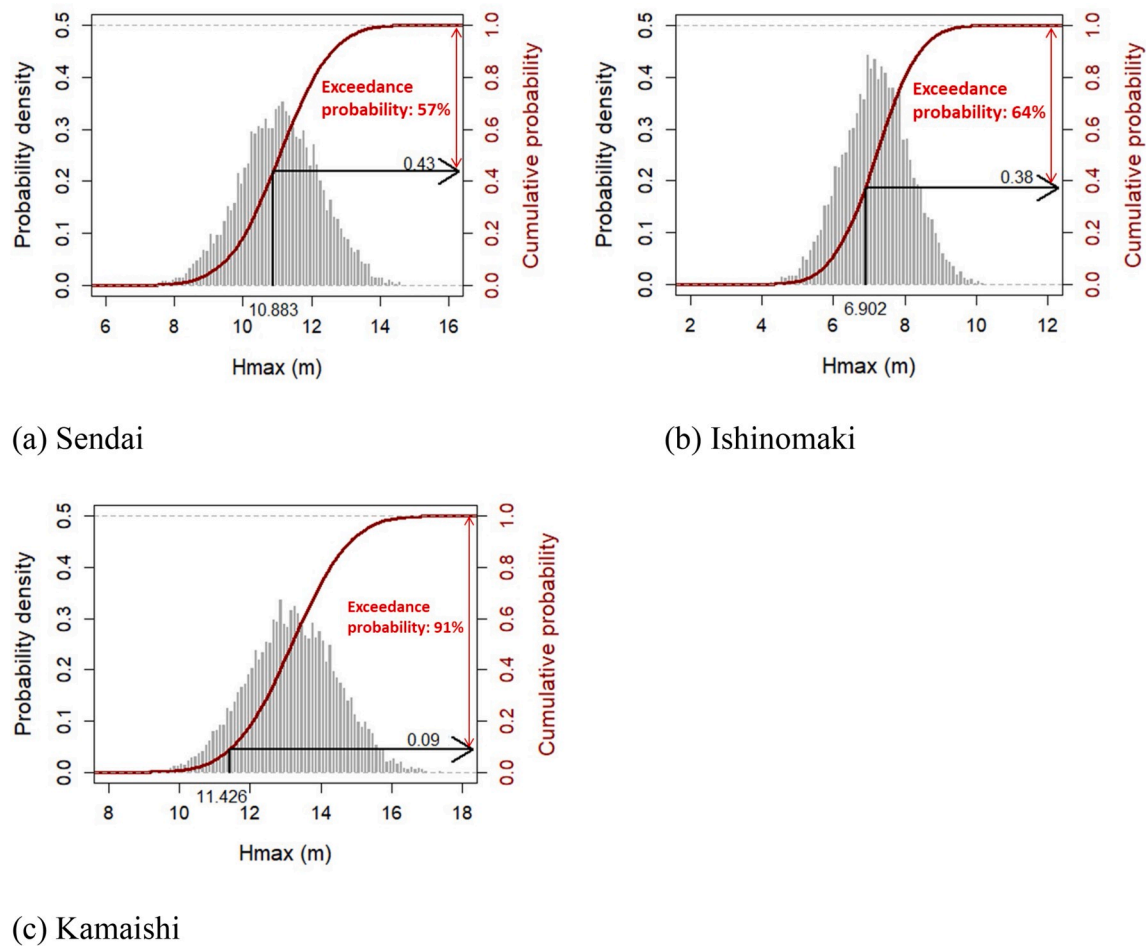


Fig. 11. Exceedance probabilities.

30%. These results can be understood in light of the fact that, as mentioned in Section 3.4.1, the fault slip is the dominant parameter for the tsunami height. In contrast, for Ishinomaki, the contribution ratio of slip is approximately 30%, while that of the modeling error is approximately 60%. This indicates that the inaccuracy of the numerical simulation at this target location contributes more to the overall uncertainty than that at the other two target locations. A possible reason for this is the effect of wave amplification near the coastline. However, to better understand this phenomenon, further investigation is needed because Kamaishi has an even more complex coastline shape than Ishinomaki.

The contribution ratios of the rake for all the target locations are relatively small. This finding is also important because the uncertainty in the rake can be less emphasized in engineering decision-making.

#### 4. Conclusion

We proposed a novel method for the response surface-based probabilistic assessment of tsunami hazards that efficiently leverages advanced numerical simulations. The method was illustrated and validated through a case study evaluating the tsunami induced by the 2011

**Table 8**

Tsunami trace heights at the target locations (2011 [Tohoku Earthquake Tsunami Joint Survey Group, 2011](#)).

	Tsunami trace height [m]	Position of tsunami trace	
		Latitude	Longitude
Sendai	12.129	38.2183	140.986
	11.203	38.2187	140.986
	9.317	38.2184	140.985
Ishinomaki	6.902	38.4139	141.287
	Kamaishi	11.426	39.2650

**Table 9**

Contribution of each source of uncertainty to the target output uncertainty.

Target point	Uncertainties (Key variables)	Variance $\sigma^2$ [m <sup>2</sup> ]	Contribution ratio [%]
Sendai	All	1.488	–
	Slip	0.904	60.7
	Rake	0.008	0.6
	Modeling error	0.580	39.0
Ishinomaki	All	0.925	–
	Slip	0.352	37.6
	Rake	0.008	0.9
	Modeling error	0.577	61.5
Kamaishi	All	1.779	–
	Slip	1.150	64.8
	Rake	0.049	2.7
	Modeling error	0.575	32.3

Great East Japan earthquake. The method was employed to estimate the exceedance probabilities with reference to the tsunami trace heights observed in a field survey and attained overall consistent results. Furthermore, we quantified the contribution ratios of different uncertainties and found that the fault slip and modeling error have much greater influences than the rake on the overall uncertainty of the tsunami height.

The key feature of the proposed method is the use of an RS obtained from a series of numerical simulations that are computationally expensive. By performing a MCS with the RS, we can efficiently estimate the probability density function of the target output. In addition, the proposed method enables us to utilize advanced numerical simulations that are computationally expensive because these simulations were needed only to construct the RSs. Furthermore, we can determine engineering priorities by estimating the contribution of each uncertainty to the target output. The proposed PTHA method is flexible and allows us to assess various tsunami risks, for example, not only tsunami heights but also inundation areas. The novel method will also be useful for assessing the tsunami risks of future earthquakes along other coastlines that have experienced tsunami-induced damage in the past.

Future work includes the extension of the proposed method to consider other uncertainties associated with tsunami hazards. Additionally, it is worth investigating adaptive RS models (e.g., [Wong et al., 2005](#)) to use an increasing number of numerical simulation runs to efficiently build a surrogate model of the numerical simulation for PTHA. Another research direction is to use the proposed approach to validate numerical models involving notable geological indicators of tsunami runup and inundation.

#### Declaration of competing interest

The authors declare that they have no known competing financial interests or personal relationships that could have appeared to influence the work reported in this paper.

#### CRedit authorship contribution statement

**T. Kotani:** Writing - original draft, Methodology. **K. Tozato:** Methodology. **S. Takase:** Methodology. **S. Moriguchi:** Conceptualization, Writing - review & editing. **K. Terada:** Supervision, Writing - review & editing. **Y. Fukutani:** Methodology. **Y. Otake:** Methodology. **K. Nojima:** Visualization. **M. Sakuraba:** Visualization. **Y. Choe:** Writing - review & editing.

#### Acknowledgments

The authors would like to gratefully acknowledge the support made through the University of Washington-Tohoku University: Academic Open Space (UW-TU:AOS).

#### References

- Aida, I., 1978. Reliability of a tsunami source model derived from fault parameters. *J. Phys. Earth* 26, 57–73. <https://doi.org/10.4294/jpe1952.26.57>.
- Akaike, H., 1973. Information theory and an extension of the maximum likelihood principle. In: Petrov, B.N., Caski, F. (Eds.), *Proceedings of the 2nd International Symposium on Information Theory*. Akademiai Kiado, Budapest, pp. 267–281.
- Amante, C., Eakins, B.W., 2009. ETOPO11 arc-minute global relief model: procedures, data sources and analysis. NOAA Technical Memorandum NESDIS NGDC-24. <https://data.nodc.noaa.gov/cgi-bin/iso?id=gov.noaa.ngdc.mgg.dem:316>.
- American Society of Civil Engineers, 2017. ASCE standard "Minimum design loads for buildings and other structures" (ASCE/SEI 7-16). <https://doi.org/10.1061/9780784414248>.
- Annaka, T., Satake, K., Sakakiyama, T., Yanagisawa, K., Shutom, N., 2007. Logic-tree approach for probabilistic tsunami hazard analysis and its applications to the Japanese coasts. In: Birkhauser Basel (Ed.), *Tsunami and Its Hazards in the Indian and Pacific Oceans*, pp. 577–592. <https://doi.org/10.1007/s00024-006-0174-3>.
- Anderson, J.G., Trifunac, M.D., 1978. Uniform risk functionals for characterization of strong earthquake ground motion. *Bull. Seismol. Soc. Am.* 68 (1), 205–218.
- Behrens, D., Dias, F., 2015. New computational methods in tsunami science. *Phil. Trans. R. Soc. A (Math. Phys. Eng. Sci.)* 373. <https://doi.org/10.1098/rsta.2014.0382>, 2053.
- Burbidge, D., Cummins, P.R., Mleczko, R., Thio, H.K., 2008. A probabilistic tsunami hazard assessment for western Australia. *Pure Appl. Geophys.* 165, 2059–2088. <https://doi.org/10.1007/s00024-008-0421-x>.
- Cornell, C.A., 1968. Engineering seismic risk analysis. *Bull. Seismol. Soc. Am.* 58 (5), 1583–1606.
- Dowson, D., Wragg, A., 1973. Maximum-entropy distributions having prescribed first and second moments (corresp.). *IEEE Trans. Inf. Theor.* 19 (5), 689–693.
- Fukutani, Y., Suppasri, A., Imamura, F., 2015. In: *Stochastic Analysis and Uncertainty Assessment of Tsunami Wave Height Using a Random Source Parameter Model that Targets a Tohoku-type Earthquake Fault*, vol. 29. *Stochastic Environmental Research and Risk Assessment*, pp. 1763–1779.
- Geist, E.L., Parsons, T., 2006. Probabilistic analysis of tsunami hazards. *Nat. Hazards* 37, 277–314.
- Goda, K., Mai, P.M., Yasuda, T., Mori, N., 2014. Sensitivity of tsunami wave profiles and inundation simulations to earthquake slip and fault geometry for the 2011 Tohoku earthquake. *Earth Planets Space* 66 (105). <https://doi.org/10.1186/1880-5981-66-105>.
- Goto, C., Ogawa, Y., 1982. *Tsunami Numerical Simulation with Leap-Frog Scheme*. Tohoku University, p. 52 (In Japanese).
- Goto, C., Ogawa, Y., Shuto, N., Imamura, F., 1997. *Numerical Method of Tsunami Simulation with the Leap-Frog Scheme (IUGG/IOC Time Project)*, IOC Manual. UNESCO.
- Grezio, A., Babeyko, A.Y., Baptista, M.A., Behrens, J., Costa, A., Davies, G., Geist, E.L., Glimsdal, S., González, F.I., Griffin, J., Harbitz, C.B., LeVeque, R.J., Lorito, S., Løvholt, F., Omira, R., Mueller, C., Paris, R., Parsons, T., Polet, J., Power, W., Selva, J., Sørensen, M.B., Thio, H.K., 2017. Probabilistic tsunami hazard analysis: multiple sources and global applications. *Rev. Geophys.* 55 (4), 1158–1198. <https://doi.org/10.1002/2017RG000579>.
- Griffin, J., Pranantyo, I.R., Kongko, W., Hauhan, A., Roniana, R., Miller, V., Davies, G., Horspool, N., Maemunah, I., Widjaja, W.B., Natawisjaja, D.H., Latief, H., 2016. In: *Assessing Tsunami Hazard Using Heterogeneous Slip Models in the Mentawai Islands, Indonesia*, vol. 441. Geological Society London Special Publications, pp. 47–70. <https://doi.org/10.1144/SP441.3>, 1.
- Hanks, T.C., Kanamori, H., 1979. A moment magnitude scale. *J. Geophys. Res.* 84 (5), 2348–2350. <https://doi.org/10.1029/JB084iB05p02348>.
- Honjo, Y., 2011. Challenges in geotechnical reliability based design. *Proceedings of the 3rd International Symp. Geotech. Safety Risk* 11–27.
- Imamura, F., Yalciner, A.C., Ozyurt, G., 2006. *Tsunami modelling manual*. <http://www.tsunami.civil.tohoku.ac.jp/hokusai3/E/projects/manual-ver-3.1.pdf>.
- Ishikawa, Y., Kameda, H., 1988. Hazard-consistent magnitude and distance for extended seismic risk analysis. In: *Proceedings of Ninth World Conference on Earthquake Engineering*. Tokyo-Kyoto, Japan, pp. 89–94.
- Japan Hydrographic Association, 2015. M7000 digital bathymetric chart, Japan nautical chart web shop. <http://www.jha.or.jp/shop/>.

- Japan Society of Civil Engineers, 2002. Tsunami assessment method for nuclear power plants in Japan. <http://committees.jsce.or.jp/ceofnp/node/>.
- Japan Society of Civil Engineers, 2011. The method of probabilistic tsunami hazard analysis (in Japanese).
- Kajiura, K., 1963. In: *The Leading Wave of a Tsunami*, vol. 41. Bulletin of the Earthquake Research Institute, University of Tokyo, pp. 535–571, 3.
- Kajiura, K., 1982. In: *Tsunami Energy in Relation to Parameters of the Earthquake Fault Model*, vol. 56. Bulletin of the Earthquake Research Institute, University of Tokyo, pp. 415–440, 3.
- Kanamori, H., 1977. The energy release in great earthquakes. *J. Geophys. Res.* 82, 2981–2987. <https://doi.org/10.1029/JB082i020p02981>.
- Larsen, B.E., Fuhrman, D.R., 2019. Full-scale CFD simulation of tsunamis. Part 1: model validation and run-up. *Coast. Eng.* 151, 22–41. <https://doi.org/10.1016/j.coastaleng.2019.04.012>.
- Lorito, S., Selva, J., Basili, R., Romano, F., Tiberti, M.M., Piatanesi, A., 2015. Probabilistic hazard for seismically induced tsunamis: accuracy and feasibility of inundation maps. *Geophys. J. Int.* 574–588. <https://doi.org/10.1093/gji/ggu408>, 200.
- McGuire, R.K., 1977. Seismic design spectra and mapping procedures using hazard analysis based directly on oscillator response. *Earthq. Eng. Struct. Dynam.* 5 (3), 211–234. <https://doi.org/10.1002/eqe.4290050302>.
- McGuire, R.K., 2004. *Seismic Hazard and Risk Analysis*. Earthquake Engineering Research Institute, Berkeley.
- Mitsoudis, D.A., Flouri, E.T., Chrysoulakis, N., Kamarianakis, Y., Okal, E.A., Synolakis, C. E., 2012. Tsunami hazard in the southeast aegean sea. *Coast. Eng.* 60, 136–148. <https://doi.org/10.1016/j.coastaleng.2011.09.004>.
- Mori, N., Goda, K., Cox, D., 2017. Recent progress in Probabilistic Tsunami Hazard Analysis (PTHA) for Mega Thrust Subduction Earthquakes. In: *The 2011 Japan Earthquake and Tsunami: Reconstruction and Restoration*. Springer, pp. 469–485.
- Mori, N., Takahashi, T., 2012. Nationwide post event survey and analysis of the 2011 Tohoku earthquake tsunami. *Coast. Eng. J.* 54, 1250001. <https://doi.org/10.1142/S0578563412500015>.
- National Research Council, 1988. *Probabilistic Seismic Hazard Analysis*. The National Academies Press, Washington, DC. <https://doi.org/10.17226/19108>.
- Necmioglu, O., Ozel, N.M., 2014. An earthquake source sensitivity analysis for tsunami propagation in the eastern mediterranean, special issue on undersea natural hazards. *Oceanography* 27 (2), 76–85. <https://doi.org/10.5670/oceanog.2014.42>.
- Okada, Y., 1992. Internal deformation due to shear and tensile faults in a half-space. *Bull. Seismol. Soc. Am.* 82 (2), 1018–1040.
- Omira, R., Baptista, M.A., Matias, L., 2015. Probabilistic tsunami hazard in the northeast atlantic from near- and far-field tectonic. *Pure Appl. Geophys.* 172, 901–920. <https://doi.org/10.1007/s00024-014-0949-9>.
- Omira, R., Matias, L., Baptista, M.A., 2016. Developing an event-tree probabilistic tsunami inundation model for NE atlantic coasts: application to a case study. *Pure Appl. Geophys.* 173, 3775–3794. <https://doi.org/10.1007/s00024-016-1367-z>.
- Park, H., Cox, D.T., 2016. Probabilistic assessment of near-field tsunami hazards: inundation depth, velocity, momentum flux, arrival time, and duration applied to Seaside, Oregon. *Coast. Eng.* 117, 79–96. <https://doi.org/10.1016/j.coastaleng.2016.07.011>.
- Park, H., Cox, D.T., Barbosa, A.R., 2018. Probabilistic Tsunami Hazard Assessment (PTHA) for Resilience Assessment of a Coastal Community. *Nat. Hazards*. <https://doi.org/10.1007/s11069-018-3460-3>.
- Park, H., Alam, M.S., Cox, D.T., Barbosa, A.R., Lindt, J.W. van de, 2019. Probabilistic seismic and tsunami damage analysis (PSTDA) for the Cascadia Subduction Zone applied to Seaside, Oregon. *Int. J. Disaster Risk Reduct.* 35, 101076. <https://doi.org/10.1016/j.ijdr.2019.101076>.
- Power, W., Downes, G., Stirling, M., 2007. Estimation of tsunami hazard in New Zealand due to south American earthquakes. *Pure Appl. Geophys.* 164, 547–564. <https://doi.org/10.1007/s00024-006-0166-3>.
- Qin, X., Motley, M.R., Marafi, N.A., 2018. Three-dimensional modeling of tsunami forces on coastal communities. *Coast. Eng.* 140, 43–59. <https://doi.org/10.1016/j.coastaleng.2018.06.008>.
- Sarfaraz, M., Park, A., 2016. SPH numerical simulation of tsunami wave forces impinging on bridge superstructures. *Coast. Eng.* 121, 145–157. <https://doi.org/10.1016/j.coastaleng.2016.12.005>.
- Sarri, A., Guillas, S., Dias, F., 2012. Statistical emulation of a tsunami model for sensitivity analysis and uncertainty quantification. *Nat. Hazards Earth Syst. Sci.* 12 <https://doi.org/10.5194/nhess-12-2003-2012>, 2003–2018, 2012.
- Satake, K., Fujii, Y., Harada, T., Namegaya, Y., 2013. Time and Space distribution of coseismic slip of the 2011 Tohoku earthquake as inferred from tsunami waveform data. *Bull. Seismol. Soc. Am.* 103, 1473–1492. <https://doi.org/10.1785/0120120122>.
- Selva, J., Tonini, R., Tiberti, M.M., Romano, F., Grezio, A., Melini, D., Piatanesi, A., Basili, R., Lorito, S., 2016. Quantification of source uncertainties in seismic probabilistic tsunami hazard analysis (SPTHA), *geophys. J. Intell.* 205, 1780–1803. <https://doi.org/10.1093/gji/ggw107>.
- Sraj, I., Mandli, K.T., Knio, O.M., Dawson, C.N., Hoteit, I., 2014. Uncertainty quantification and inference of Manning's friction coefficients using DART buoy data during the To hoku tsunami. *Ocean Model.* 83, 82–97.
- Stefanakis, T.S., Contal, E., Vayatis, N., Dias, F., Synolakis, C.E., 2014. Can small islands protect nearby coasts from tsunamis? An active experimental design approach. In: *Proceedings of the Royal Society A: Mathematical, Physical and Engineering Sciences*, vol. 470. Royal Society publishing, p. 20140575. <https://doi.org/10.1098/rspa.2014.0575>.
- Suppasri, A., Imamura, F., Koshimura, S., 2012. Probabilistic tsunami hazard analysis and risk to coastal populations in Thailand. *J. Earthq. Tsunami* 6 (2), 1250011. <https://doi.org/10.1142/S179343111250011X>.
- The Port and Airport Research Institute, Nationwide Ocean Wave information network for Ports and Harbours (NOWPHAS), <http://nowphas.mlit.go.jp/nowphasdata/static/sub311.htm>.
- Thio, H.K., Somerville, P., Ichinose, G., 2007. Probabilistic analysis of strong ground motion and tsunami hazards in Southeast Asia. *J. Earthq. Tsunami* 1 (2), 119–137. <https://doi.org/10.1142/S1793431107000080>.
- Tohoku Earthquake Tsunami Joint Survey Group, 2011. Nationwide field survey of the 2011 off the pacific coast of Tohoku earthquake tsunami. *J. Jpn. Soc. Civ. Eng. Ser. B2 (Coast. Eng.)* 67, 63–66. <https://doi.org/10.2208/kaigan.67.63>.
- Volpe, M., Lorito, S., Selva, J., Tonini, R., Romano, F., Brizuela, B., 2019. From regional to local SPTHA: efficient computation of probabilistic tsunami inundation maps addressing near-field sources. *Nat. Hazards Earth Syst. Sci.* 19, 455–469. <https://doi.org/10.5194/nhess-19-455-2019>.
- Wong, S.M., Hobbs, R.E., Onof, C., 2005. An adaptive response surface method for reliability analysis of structures with multiple loading sequences. *Struct. Saf.* 27 (4), 287–308. <https://doi.org/10.1016/j.strusafe.2005.02.001>.
- Working Group on California Earthquake Probabilities, 1995. *Seismic hazards in southern California - probable earthquakes, 1994 to 2024*. *Bull. Seismol. Soc. Am.* 85, 379–439.